Insect Molecular Biology

Insect Molecular Biology (2016) **00**(00), 00–00 doi: 10.1111/imb.12285

Validation of ADAM10 metalloprotease as a *Bacillus thuringiensis* Cry3Aa toxin functional receptor in Colorado potato beetle (*Leptinotarsa decemlineata*)

V. M. Ruiz-Arroyo*, I. García-Robles*, C. Ochoa-Campuzano*, G. A. Goig*, E. Zaitseva†‡, G. Baaken‡, A. C. Martínez-Ramírez§, C. Rausell*[1] and M. D. Real*[1]

**Department of Genetics, University of Valencia, Burjassot, Valencia, Spain;* †*Department of Physiology, University of Freiburg, Freiburg, Germany;* ‡*Ionera Technologies GmbH, Freiburg, Germany; and* §*Servicios Centrales de Soporte a la Investigación Experimental (SCSIE), University of Valencia, Burjassot, Valencia, Spain*

Abstract

Bacillus thuringiensis **parasporal crystal proteins (Cry proteins) are insecticidal pore-forming toxins that bind to specific receptor molecules on the brush border membrane of susceptible insect midgut cells to exert their toxic action. In the Colorado potato beetle (CPB), a coleopteran pest, we previously proposed that interaction of Cry3Aa toxin with a CPB ADAM10 metalloprotease is an essential part of the mode of action of this toxin. Here, we annotated the gene sequence encoding an ADAM10 metalloprotease protein (CPB-ADAM10) in the CPB genome sequencing project, and using RNA interference gene silencing we demonstrated that CPB-ADAM10 is a Cry3Aa toxin functional receptor in CPB. Cry3Aa toxicity was significantly lower in CPB-ADAM10 silenced larvae and** ***in vitro*** **toxin pore-forming ability was greatly diminished in lipid planar bilayers fused with CPB brush border membrane vesicles (BBMVs) prepared from CPB-ADAM10 silenced larvae. In accordance with our previous data that indicated this toxin was a substrate of ADAM10 in CPB, Cry3Aa toxin membrane-associated proteolysis was altered when CPB BBMVs lacked ADAM10. The functional validation of CPB-ADAM10 as a Cry3Aa toxin receptor in CPB expands the already recognized role of ADAM10 as a pathogenicity determinant of pore-forming toxins in humans to an invertebrate species.**

Keywords: ***Bacillus thuringiensis*****, ADAM10 metalloprotease, Cry3Aa toxin, Colorado potato beetle.**

Correspondence: Carolina Rausell or M. Dolores Real, Department of Genetics, University of Valencia, C/ Doctor Moliner 50, 46100-Burjassot, Valencia, Spain. Tel.: 34-963543397; e-mails: carolina.rausell@uv.es; maria.dolores.real@uv.es

[1]These authors contributed equally to this work.

Introduction

The gut epithelium constitutes a functional barrier to microorganisms and foreign antigens but many bacteria have evolved diverse mechanisms to overcome host defences, and thereby exert a pathogenic effect. Pore-forming toxins (PFTs) are one of the most widespread bacterial virulence factors, comprising about 25 to 30% of all cytotoxic bacterial proteins (Los *et al*., 2013). Despite the great variety of sequences and structures amongst PFTs, they all share a common mode of action. Most PFTs are produced as precursor monomeric toxins that interact with specific receptors in the target membrane promoting toxin oligomerization and membrane insertion, leading to pore formation (Bischofberger *et al*., 2012). Interaction of PFTs with several host cell proteinaceous receptors such as glycosylphosphatidylinositol (GPI)-anchored proteins, cadherins, ADAM10 and C-C chemokine receptor type 5 (CCR5) or lipidic receptors including cholesterol and glycolipids has been reported (Gordon *et al*., 1999; Abrami *et al*., 2002; Piggot & Ellar, 2007; Wilke & Bubeck Wardenburg, 2010; Alonzo *et al*., 2013). Some PFTs require activation by proteolytic cleavage or additional cofactors, but all PFTs perforate the membrane of host cells, forming either small or large pores. The secondary structure of the region that inserts into the membrane classifies PFTs into two categories, α-PFTs, such as *Escherichia coli* colicins or *Bacillus thuringiensis* (Bt) Cry toxins, and β-PFTs, the majority of bacterial PFTs, such as *Aeromonas hydrophila* aerolysin

and *Staphylococcus aureus* α-toxin, depending on whether the secondary structures are α-helices or β-barrels, respectively (Dal Peraro & van der Goot, 2016).

During sporulation, the Gram-positive bacterium Bt produces α-PFT insecticidal Cry proteins that bind specific receptor molecules on the brush border membranes of the insect midgut cells. Bt toxin-receptor interaction is widely accepted as a crucial step for toxicity and determines insect specificity (Pigott & Ellar, 2007). The best-characterized Bt toxin receptors are cadherin-like, and the GPI-anchored aminopeptidase-N and alkaline phosphatase molecules, although other candidates, such as glycolipids and membrane transporters, have been reported in several insect orders and nematodes (Adang *et al*., 2014).

In the devastating coleopteran pest *Leptinotarsa decemlineata* (Colorado potato beetle, CPB), we reported that Cry3Aa toxin interacts with ADAM-like membrane-associated metalloproteases in the CPB midgut through a region of the toxin domain II, and that it is proteolytically processed in regions of the toxin domain III (Ochoa-Campuzano *et al*., 2007; Rausell *et al*., 2007). We also demonstrated that the interaction between toxin domain II and ADAM is required for Cry3Aa membrane associated cleavage by ADAM and is a significant determinant of the insecticidal activity of this toxin against CPB (García-Robles *et al*., 2012).

"A Disintegrin And Metalloproteases" (ADAMs) proteases superfamily belong to the metzincin subgroup of the zinc proteases and are widely present from protozoans to mammals. ADAMs are modular transmembrane proteins that have been found to be key regulators of important biological processes, functioning as cellular sheddases of various membrane-associated proteins such as cytokines and growth factors, receptors and their ligands, and cell adhesion and fusion molecules. They are involved in multiple developmental processes, cell–cell interaction and migration, and signalling. Therefore, dysregulation of ADAM function results in a broad spectrum of pathologies such as autoimmune and cardiovascular diseases, neurodegeneration, infection, inflammation and cancer (Reiss & Saftig, 2009). Increased ectodomain shedding as a result of ADAM activation has been reported in cells attacked by PFTs (Reiss & Bhakdi, 2012). Interestingly, *S. aureus* α-haemolysin injures epithelial cells by interacting with the ADAM10 receptor (Wilke & Bubeck Wardenburg, 2010; DuMont & Torres, 2014), which facilitates toxin oligomerization and subsequent pore formation (Berube & Bubeck Wardenburg, 2013).

In this work, we searched the *ADAM10* gene sequence in the CPB genome that is currently being annotated (Lee *et al*., 2013), and we contributed these data to the insect genome project (i5k; https://www.hgsc.bcm.edu/arthropods/colorado-potato-beetle-genome-project). We then assessed the functional role of the corresponding protein in the Cry3Aa toxin's mode of action in CPB larvae by RNA interference (RNAi) gene silencing, and we investigated the involvement of CPB ADAM10 metalloprotease in Cry3Aa toxin membrane-associated proteolysis and pore formation.

Results

Functional annotation of an ADAM10 gene in the CPB genome

Previously, we proposed that an ADAM10 metalloprotease (CPB-ADAM10) is essential in the Cry3Aa toxin's mode of action against CPB larvae (Ochoa-Campuzano *et al*., 2007). In the present work, to validate CPB-ADAM10 protein as a Cry3Aa toxin functional receptor we assessed the effect of expression knockdown of the corresponding gene in the insecticidal activity of Cry3Aa toxin against CPB larvae.

The *CPB-ADAM10* gene nucleotide sequence is not available in public databases but, as the CPB genome is being annotated, to look for CPB gene sequence orthologues of ADAM10 from *Tribolium castaneum* [TcADAM10, National Center for Biotechnology Information (NCBI) accession number: XM_008199908] we performed a BLAST-like alignment tool (BLAT) search on the Apollo annotation server.

The BLAT analysis with predicted TcADAM10 mRNA (XM_008199908) yielded several reads in scaffold 927, but a full *CPB-ADAM10* gene sequence could not be assembled, as many gaps are currently present in this genome region. We designed PCR primers to fill in the gap area and to complete the 5′-end of the coding sequence by a 5′ rapid amplification of cDNA ends (5′-RACE) reaction (Fig. S1). Then, we resequenced the full *CPB-ADAM10* coding sequence (Fig. S2) and deposited it in the NCBI database (accession number: KX388389). The *CPB-ADAM10* mRNA is 2640 bp long, encoding a 904-amino-acid protein with a predicted molecular mass of 101.38 kDa and a calculated isoelectric point (pI) of 7.78 estimated with the pI/Mw tool on the ExPASy server (Gasteiger *et al*., 2005). Using TMHMM (Krogh *et al*., 2001), a large extracellular domain [amino acids (aa): 1–769], a transmembrane region (aa: 770–789) and a short cytosolic domain (aa: 795–904) were identified. Using InterProScan (Jones *et al*., 2014), typical ADAM motifs were found in the extracellular domain, including a signal sequence (aa: 1–20), a propeptide domain (aa: 46–158), a metalloprotease domain (aa: 268–535), a disintegrin domain (aa: 539–644) and a cysteine-rich region (aa: 645–671) (Fig. 1A). Comparison of the deduced amino acid sequence of the CPB-ADAM10 protein with that of the human ADAM10 protein revealed a 43% amino acid sequence identity and the same domain organization (Fig. S3).

A molecular phylogenetic tree was constructed including several insect orders, *Xenopus laevis* and human ADAM10

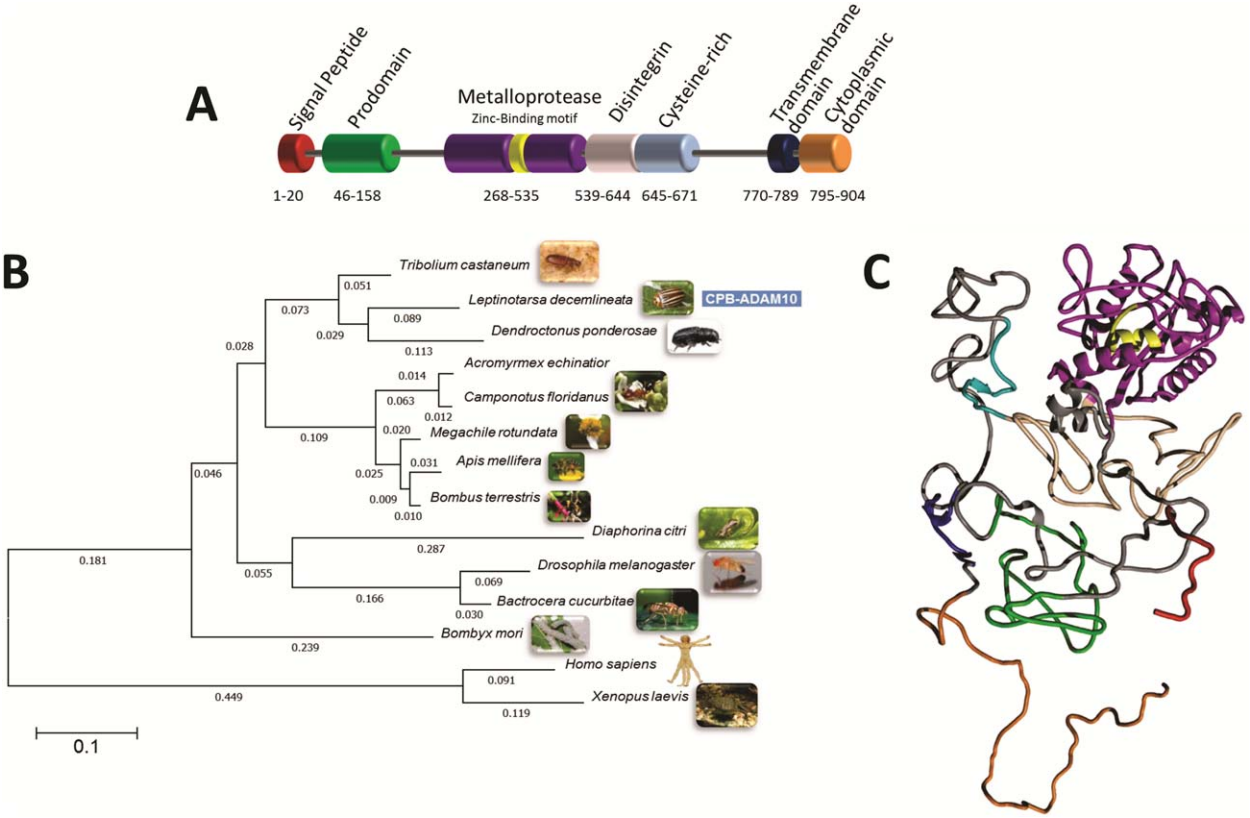

Figure 1. Colorado potato beetle-ADAM10 metalloprotease (CPB-ADAM10) protein. (A) Schematic representation of the domain organization of CPB-ADAM10 metalloprotease's secondary structure obtained with InterProScan (Jones *et al*., 2014) showing the extracellular domain containing a signal peptide, a prodomain, the metalloprotease catalytic site (including the zinc-binding motif), a disintegrin domain and a cysteine-rich region, followed by the transmembrane region and the cytosolic tail. (B) Unrooted phylogenetic tree generated with Mega 5 (http://www.megasoftware.net) (Tamura *et al*., 2011) of 12 insect ADAM10 protein sequences (including the CPB-ADAM10 protein sequence) and the *Homo sapiens* and *Xenopus laevis* ADAM10 sequences. The neighbour-joining method (Saitou & Nei, 1987) was used to construct the phylogenetic tree. The tree is drawn to scale, with branch lengths in the same units as those of the evolutionary distances used to infer the phylogenetic tree. The evolutionary distances were computed using the Poisson correction method (Zuckerkandl & Pauling, 1965) and are in the units of the number of amino acid substitutions per site. Most of the organisms' pictures are from Wikimedia Commons and the authors are credited with authorship in Fig. S4. (C) Representation of the three-dimensional model of CPB-ADAM10 metalloprotease created using the I-TASSER server (Roy *et al*., 2010). Colours were assigned using PyMOL (Delano Scientific Inc, Palo Alto, CA, USA) and correspond to those used in the schematic representation of the domain organization in (A).

protein sequences (Fig. 1B). CPB-ADAM10 clustered together in one group with the coleopteran insects *T. castaneum* and *Dendroctonus ponderosae*, sharing sequence identities of 78 and 75%, respectively. As expected, the human and *X. laevis* ADAM10 proteins were far apart from the rest of the ADAM10 proteins.

We also predicted the three-dimensional model of the CPB-ADAM10 protein using the I-TASSER software (Roy *et al*., 2010). As seen in Fig. 1C, the model exhibits the same overall structure as other ADAM10 metalloprotease proteins.

ADAM10 is a Cry3Aa toxin functional receptor in CPB larval midgut

Once the *CPB-ADAM10* gene sequence was functionally annotated, we assessed the effect of expression knockdown of this gene in Cry3Aa toxin's insecticidal activity against CPB larvae. To choose the appropriate larval size for silencing, we obtained the transcription profile of the *CPB-ADAM10* gene during CPB larval development by quantitative real-time PCR (qRT-PCR; Fig. 2A), using the ribosomal protein 4 (*RP4*) gene as an internal control because it has been described as a stable reference gene in CPB (Zhu *et al*., 2011). As the *CPB-ADAM10* gene expression profile remained almost constant through larval development, for RNAi experiments we selected larvae in a weight range of 15–23 mg that allowed toxicity assays to be performed following silencing, so that pupation was not reached during the time course of the bioassay. Transcript abundance was reduced by 73% in the *CPB-ADAM10* gene expression knockdown assays (Fig. 2B).

We next performed toxicity assays with Cry3Aa toxin on double-stranded RNA (dsRNA) treated and

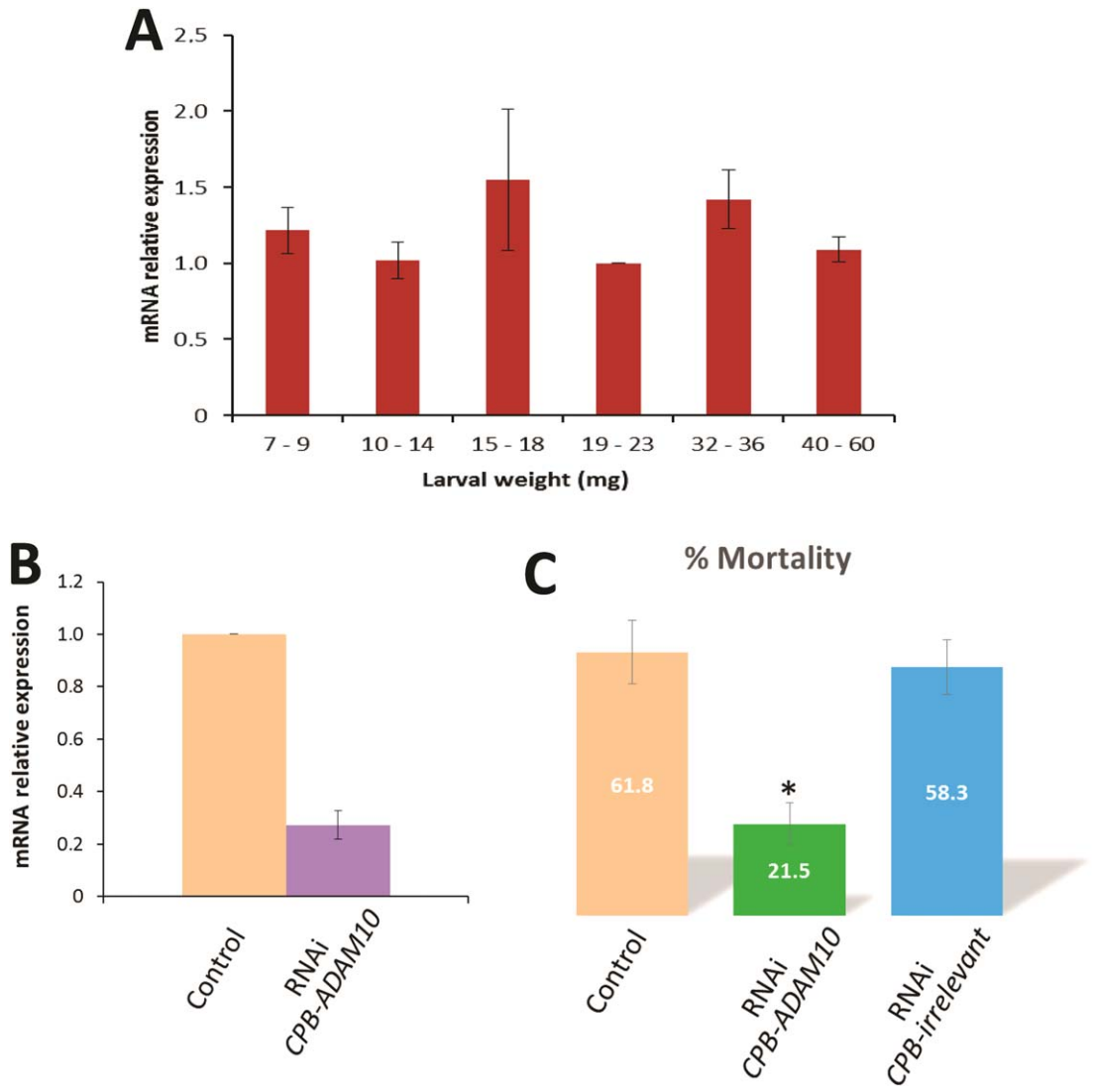

Figure 2. Colorado potato beetle-ADAM10 metalloprotease (CPB-ADAM10) is a Cry3Aa toxin functional receptor. (A) mRNA expression levels of the *CPB-ADAM10* gene in CPB midguts as a function of larval weight. The relative amount of CPB transcripts obtained by quantitative real-time PCR (qRT-PCR) analysis using the ribosomal protein 4 (*RP4*) gene as reference was compared to the mRNA amount corresponding to 19–23 mg larval weight. Error bars indicate standard errors of the means from two biological replicates of six individuals per replicate. (B) RNA interference (RNAi) gene silencing in CPB larvae in response to ingestion of *CPB-ADAM10* double-stranded RNA (dsRNA). The relative amount of CPB gene transcripts estimated by qRT-PCR and normalized to the expression of the *RP4* gene was compared in control and silenced larvae. The statistical significance of gene expression between the two samples was evaluated using Student's *t*-test, and significant knockdown was observed ($P < 0.05$). The error bars represent standard errors of the mean of three biological samples of six individuals per replicate and three technical replicates each. (C) Mortality percentage following Cry3Aa toxin treatments on either control or RNAi-silenced larvae. Mortality experiments were performed using 16 silenced CPB larvae and the corresponding controls. A CPB-irrelevant dsRNA (Fig. S5) synthesized using primers constructed at random, without any predetermined sequence, was included. Error bars represent standard error of the mean of at least two biological replicates. The asterisk indicates that the mortality decrease observed upon Cry3Aa toxin ingestion in silenced larvae with respect to toxin-challenged control larvae was statistically significant using Student's *t*-test ($P < 0.05$).

nontreated control larvae (Fig. 2C). *CPB-ADAM10* dsRNA silenced larvae challenged with Cry3Aa toxin showed a statistically significant 65% mortality reduction compared with nonsilenced larvae or larvae treated with an irrelevant dsRNA derived from primers constructed at random (Student's *t*-test, $P < 0.05$). This is consistent with CPB-ADAM10 protein being required for Cry3Aa-mediated toxicity.

CPB-ADAM10 is involved in Cry3Aa toxin pore formation and Cry3Aa toxin membrane-associated proteolysis

To confirm that CPB-ADAM10 is essential for toxin-induced membrane permeabilization, as expected for a Cry toxin functional receptor, we investigated the toxin's pore-forming activity in lipid bilayers fused with brush border membrane vesicles (BBMVs) from control larvae, BBMVs from CPB-ADAM10 silenced larvae and in pure

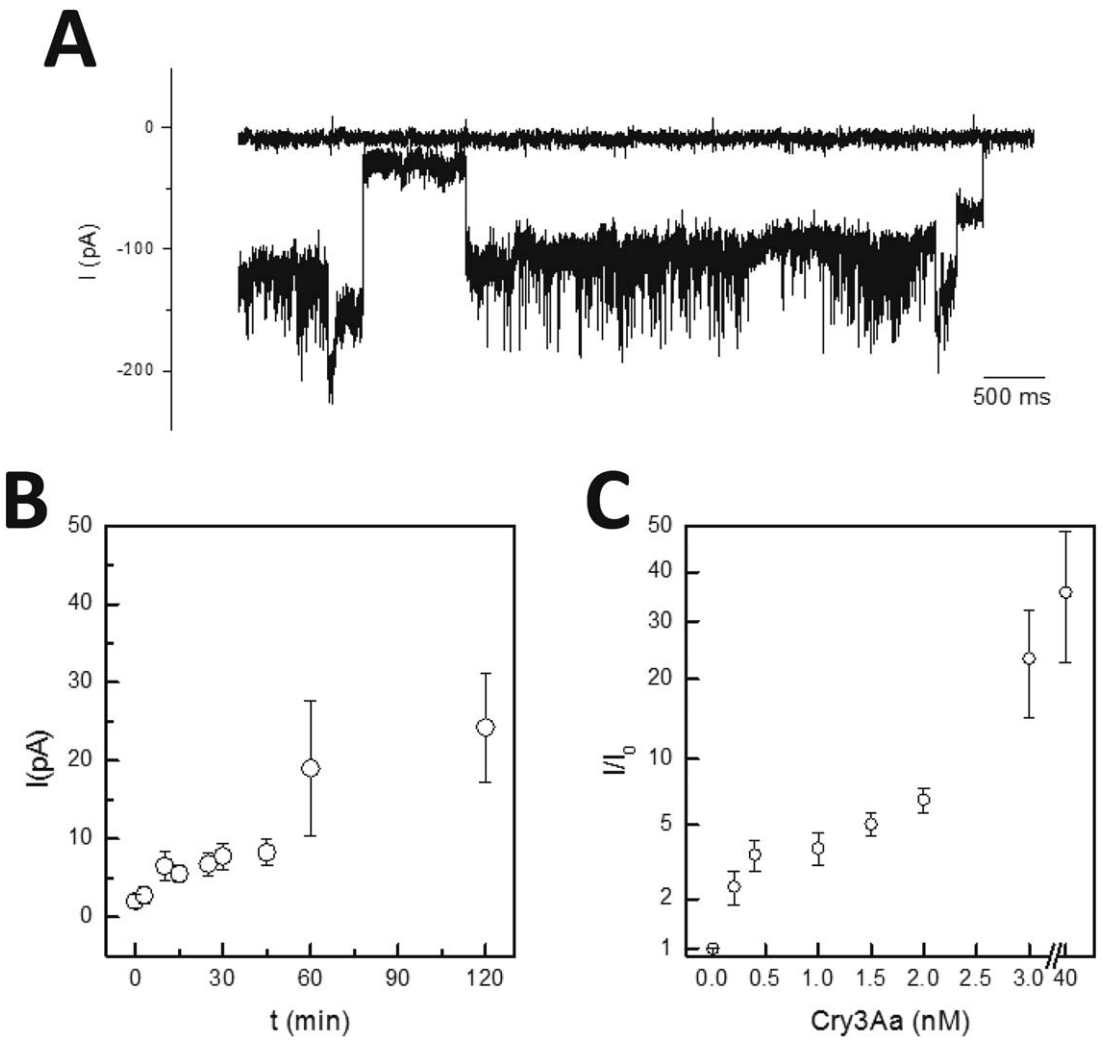

Figure 3. Cry3Aa toxin forms pores in lipid planar bilayers fused with Colorado potato beetle brush border membrane vesicles (CPB BBMVs). (A) Representative traces illustrating Cry3Aa toxin pores in a lipid bilayer with fused control BBMVs. Upper trace: current recording prior to the addition of toxin; lower trace 60 min after addition of 2 nM Cry3Aa toxin; holding potential −50 mV. (B) Changes in the average membrane current over time after addition of Cry 3A toxin (2 nM), reflecting multiple pore insertions in membranes with fused control BBMVs. Displayed are the mean values of four independent measurements together with standard errors. Average current values were calculated from 60-s macroscopic current recordings at holding potential of 30 mV. (C) Normalized average current values recorded at different Cry3Aa toxin concentrations in membranes with fused control BBMVs. Displayed are the mean values from 15 bilayers together with standard errors. Currents are averages from 60-s recordings at holding potential of 30 mV after approximately 30 min incubation with the toxin. I, recorded current value; I_0, current value recorded before the addition of the toxin.

synthetic lipid membranes. BBMVs fuse spontaneously with planar lipid bilayers leading to the incorporation of different types of membrane proteins and endogenous ion channels present in the midgut epithelial membrane into the lipid bilayers (Martin & Wolfersberger, 1995; Peyronnet *et al.*, 2001). The fusion of BBMVs with the bilayer array on a micro electrode cavity array (MECA) chip resulted in the appearance of ionic currents of different amplitudes owing to the incorporation of endogenous channels. Addition of the Cry3Aa toxin to the bilayers fused with BBMVs from control larvae induced in approximately 70% of the membranes pronounced changes in the membrane currents owing to the toxin pore formation already in low nM concentrations after several minutes of incubation (Fig. 3). Figure 3A shows representative recordings before and 60 min after incubation with 2 nM of Cry3Aa toxin.

As channel activity varied greatly from one bilayer to another owing to the variable number of inserted channels, average currents were calculated for the further characterization of Cry3Aa toxin pore formation. Figure 3B illustrates changes in average membrane current resulting from multiple Cry3Aa pore insertions during incubation of receptor-containing bilayers with the toxin. The presence of the CPB-ADAM10 receptor in the fused control BBMVs allowed for detection of channel activity

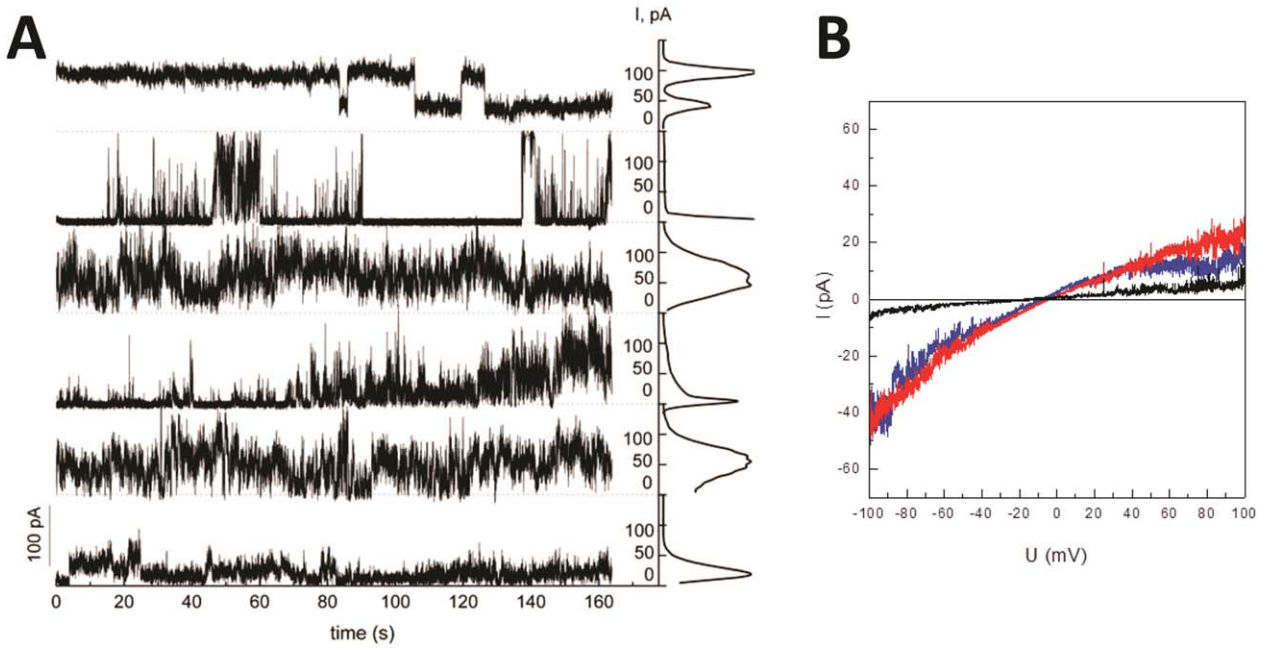

Figure 4. Representative recordings from Cry3Aa channels in pure synthetic lipid bilayers on the micro electrode cavity array chip illustrating the diversity of the channels. (A) Parallel current recordings from six lipid bilayers with inserted Cry3Aa channels at 100 mV together with corresponding normalized all point histograms. Cry3Aa toxin concentration 100 nM. (B) Current (I)-voltage (U) traces of selected stable Cry3A toxin channels under a ramping voltage of −100/+100 mV.

at toxin concentrations as low as 0.5 nM (Fig. 3C), whereas in the fused CPB-ADAM10 silenced BBMVs Cry3Aa pore formation was only observed at toxin concentrations above 14.5 nM (data not shown). Similarly high toxin concentrations were needed to induce pores in pure synthetic lipid membranes. Figure 4 shows simultaneous recording of the currents from six diphytanoyl-phosphocholine (DPhPC) bilayers induced by incubation with 100 nM toxin together with the corresponding current amplitude histograms.

Detailed analysis of the Cry3Aa single-channel conductance levels was difficult because most of the pores displayed a variable kinetic behavior with low channel open probability, complex activity patterns and multiple subconductance states typically observed for Cry proteins (Gómez *et al.*, 2014). Stable pores with high open probability and single-channel transition steps ranging from 200 to 800 pS were recorded in synthetic receptor-free planar lipid bilayers in only 17 cases. Such channels were typically observed after bilayer disruption and reformation at very high toxin concentrations (20–300 nM). The current–voltage relationships of three of these stable channels are shown in Fig. 4B. Taken together, these results indicate that the CPB-ADAM10 protein is required for efficient Cry3Aa toxin pore formation.

Previously, we demonstrated that when CPB-ADAM10 interaction with Cry3Aa toxin through loop I of the toxin domain II was prevented, not only Cry3Aa toxin pore formation was significantly reduced but also toxin membrane-associated proteolysis (Ochoa-Campuzano *et al.*, 2007). As shown in Fig. 5, upon incubation with BBMVs from *CPB-ADAM10* silenced larvae, Cry3Aa toxin was cleaved although the proteolytic profile was different than that obtained from incubation with nonsilenced CPB BBMVs. Whereas the protein bands higher than 40 kDa were the same in both lanes, cleavage fragments of 35, 30 and 27 kDa were absent in Cry3Aa toxin proteolysed by BBMVs from *CPB-ADAM10* silenced larvae, and a new 28.5-kDa protein band appeared. These results corroborate that CPB-ADAM10 metalloprotease participates in the midgut epithelial membrane associated Cry3Aa toxin proteolytic processing.

Discussion

The sequencing of entire microbial genomes and their hosts together with multidisciplinary efforts to study bacterial pathogenesis are expanding our knowledge on the molecular basis of the mode of action of PFTs. In this study, we used CPB genomic data for functional annotation of the *CPB-ADAM10* gene, a putative Cry3Aa receptor in this insect. The corresponding protein sequence exhibited the conserved domain structure of ADAM metalloproteases (Fig. 1A). *CPB-ADAM10* gene expression was detected throughout larval development (Fig. 2A). Consistent with this finding, in the data set of

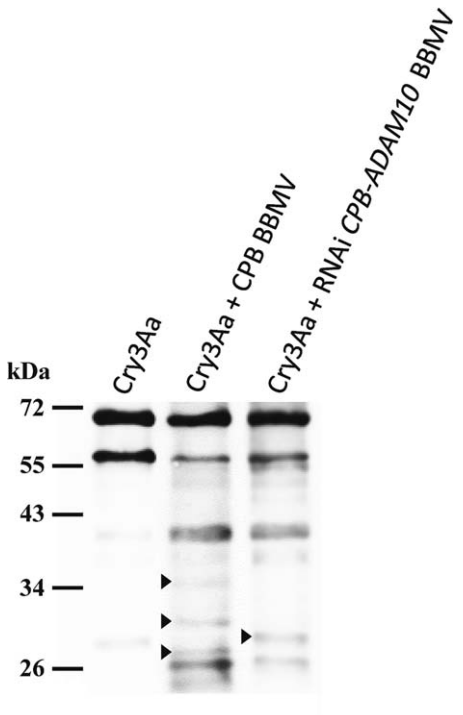

Figure 5. Analysis of Colorado potato beetle brush border membrane vesicle (CPB-BBMV) proteolytic activity on the Cry3Aa toxin. Polypeptide profile of the Cry3Aa toxin cleaved by CPB-BBMV proteases from nonsilenced control larvae (lane Cry3Aa + CPB BBMV) and Colorado potato beetle-ADAM10 metalloprotease (CPB-ADAM10) silenced larvae (lane Cry3Aa + RNAi CPB-ADAM10 BBMV) obtained by western blotting analysis with a polyclonal anti-Cry3Aa antibody. Arrow heads point to bands that were distinctive of each lane. The Cry3Aa toxin is shown on the left. Abbreviation: RNAi, RNA interference.

the CPB larvae transcriptomic analysis carried out by Pauchet *et al*. (2010) (Sequence Read Archive (SRA) GenBank link: SRX017239), we identified 22 transcript fragments corresponding to ADAM10 metalloprotease.

As orally delivered dsRNA works very efficiently for RNAi gene silencing in most beetle species, especially in CPB (Palli, 2014), we employed this technique to examine the involvement of the CPB-ADAM10 protein in Cry3Aa toxin's mode of action. Our results confirmed that CPB-ADAM10 is a Cry3Aa functional receptor in CPB, as we previously proposed (Ochoa-Campuzano *et al*., 2007). First, Cry3Aa toxicity was significantly lower in *CPB-ADAM10* silenced larvae (Fig. 2), as expected for a toxin receptor. Second, *in vitro* toxin pore-forming ability was greatly diminished in lipid planar bilayers fused with CPB BBMVs prepared from *CPB-ADAM10* silenced larvae (Figs (3 and 4)), which supports Cry3Aa toxin interaction with CPB-ADAM10 is required for membrane permeabilization. Third, Cry3Aa toxin membrane-associated proteolysis was altered when CPB BBMVs lacked ADAM10 (Fig. 5), in accordance with our previous data that indicated this toxin is a substrate of ADAM10 in CPB (Ochoa-Campuzano *et al*., 2007; García-Robles *et al*., 2012).

Previously, we reported the interaction of the Cry3Aa toxin with ADAM-like membrane-associated metalloproteases in the midgut of CPB larvae through a specific recognition sequence in the toxin domain II, which results in the toxin being proteolytically processed in regions of domain III (Ochoa-Campuzano *et al*., 2007; Rausell *et al*., 2007). It has been described that the catalytic site of ADAM10 is shielded by the disintegrin/Cys-rich domain and it has been proposed that this site is exposed by enzyme structural changes triggered by substrate interactions distal to the cleavage site (Takeda, 2009; Hartman *et al*., 2013). The function of CPB-ADAM10 as a mediator of Cry3Aa toxin susceptibility is complex because of the dual role of the Cry3Aa toxin as a CPB-ADAM10 interacting protein and CPB-ADAM10 proteolysis substrate. When the Cry3Aa toxin recognition site on CPB-ADAM10 was blocked (Ochoa-Campuzano *et al*., 2007) or when CPB-ADAM10 was absent (this work), Cry3Aa toxin pore-forming activity was significantly diminished. However, when CPB-ADAM10 was present but the metalloprotease catalytic activity was inhibited, Cry3Aa toxin pore formation was enhanced (Rausell *et al*., 2007). Therefore, although the interaction with ADAM10 through the Cry3Aa recognition motif is essential for Cry3Aa membrane permeabilization, at the same time, ADAM10 metalloprotease cleaves Cry3Aa, rendering the toxin less efficient for pore formation.

To date, ADAM10 metalloprotease has not been reported to be involved in the mode of action of any other Bt Cry toxin, but very interestingly it has been reported to be a cellular receptor for *S. aureus* α-toxin (Wilke & Bubeck Wardenburg, 2010). The α-toxin-ADAM10 complex facilitates toxin membrane binding with subsequent oligomerization and pore formation leading to host cell signalling and cellular lysis. The formation of toxin pores enhances the proteolytic activity of ADAM10, leading to increased E-cadherin ectodomain shedding that causes further disruption of the epithelial barrier's function by dismantling adherens junctions (Berube & Bubeck Wardenburg, 2013). *Streptococcus pneumoniae* pneumolysin also induced ADAM10-mediated E-cadherin cleavage (Inoshima *et al*., 2011). Therefore, it has been suggested that ADAM10 may be utilized by multiple PFTs for pathological E-cadherin cleavage (Inoshima *et al*., 2011; Berube & Bubeck Wardenburg, 2013). Generalization and cross-species translation of PFTs' functions in pathogenesis has been claimed by scientists in the field as a means for better understanding the pathogenic mechanisms of this group of bacterial toxins that will allow focusing on the common grounds of PFTs–host interactions (Los *et al*., 2013).

Interestingly, E-cadherin-like proteins in the midgut of larvae susceptible to Cry toxins have been reported to mediate toxicity in many insects of several orders by acting as Cry toxin receptors (Pigott & Ellar, 2007; Adang *et al.*, 2014). In the order Coleoptera, it has been reported that cadherin-like proteins act as Cry3 toxin functional receptors in *Tenebrio molitor*, *T. castaneum* and *Alphitobius diaperinus* (Fabrick *et al.*, 2009; Contreras *et al.*, 2013; Hua *et al.*, 2014). For this reason, the CPB-Cry3Aa PFT tandem emerges as an amenable system for cross-species translation of the *in vivo* role of ADAM10 to clarify the effects by which PFTs compromise the integrity of the epithelial membrane bilayer.

Experimental procedures

Bt Cry toxin purification

Cry3Aa crystals were produced in Bt strain BTS1. Crystal inclusions were separated from spores and cell debris by centrifugation on discontinuous 67, 72, 79 and 84% weight/volume (w/v) sucrose gradients in 50 mM Tris–HCl, pH 7.5, as described by Thomas & Ellar (1983). Crystal proteins were solubilized in 50 mM Na_2CO_3, pH 10.5, for 2 h at 37 °C. Purity of the crystal preparation was monitored by phase contrast microscopy and analysed by 10% sodium dodecyl sulphate polyacrylamide gel electrophoresis (SDS-PAGE). Protein concentration was measured by the protein-dye method of Bradford (1976), using Bovine Serum Albumin (BSA) as a standard.

Insects

A laboratory colony of *L. decemlineata* (CPB) founded from eggs collected from fields located in Valencia and Granada (Spain) was used. Larvae and adults were reared on greenhouse-grown potato plants at 25 ± 1 °C and with a photoperiod of 16:8 h (light : dark). Fresh leaves were supplied to the larvae every 24 h.

RNA isolation and cDNA synthesis

Total RNA was isolated from six dissected midguts of second-instar CPB larvae using TRIZOL LS Reagent (Life Technologies, Rockville, MD, USA), following the manufacturer's protocol, and the purified RNA was treated with DNase I (Takara, Kyoto, Japan). RNA was precipitated in 10 M ammonium acetate, pH 7.0, and absolute ethanol at −20 °C for 12 h. After centrifugation, the sediment was resuspended in RNase free H_2O (Sigma, St Louis, MO, USA) and stored at −85 °C for further assays. RNA quality was assessed by 1% agarose gel electrophoresis and quantification was carried out with a spectrophotometer (ThermoScientific™ NanoDrop 2000, ThermoFisher Wilmington, DE, USA). The GoScript Reverse Transcription System (Promega, Madison, WI, USA) was used for cDNA synthesis according to the manufacturer's protocol using oligo-dT and random hexamers.

dsRNA synthesis

cDNA was used as template for PCR amplification using PrimeSTAR polymerase (Takara) and specific primers containing a T7 polymerase promoter sequence at their 5′ end generated from the *CPB-ADAM10* gene sequence (Table 1). As a control, a dsRNA was synthesized, in the same conditions as described above, using primers constructed at random, without any predetermined sequence (T7 CPB-irrelevant dsRNA, Table 1). The PCR products were used for *in vitro* dsRNA transcription using an AmbionMEGAscript T7 kit (Applied Biosystems, Foster City, CA, USA) according to the manufacturer's protocol. Purified dsRNA was stored at −20 °C until administered to CPB larvae in RNAi gene-silencing experiments.

qRT-PCR

To analyse the expression of the *CPB-ADAM10* gene during larval development, qRT-PCR amplification was performed on RNA obtained from groups of six larvae of different weights within a range of 7–60 mg. cDNA synthesis was performed as described in the 'RNA isolation and cDNA synthesis' section. qRT-PCR amplification was performed using Power SYBR Green PCR Master Mix (Applied Biosystems), 10 ng cDNA, and gene-specific forward (F) and reverse (R) primers (Table 1), designed with Primer3Plus software (Untergasser *et al.*, 2007). A StepOnePlus Real-Time PCR system (Applied Biosystems) was used, under the conditions recommended by the manufacturer. For each experiment, two biological replicates were analysed using the mean values of three technical replicates. Relative-fold calculations were made using ribosomal protein *RP4* as the reference gene (Table 1) to normalize gene expression as reported by Zhu *et al.* (2011). Data were analysed by Student's *t*-tests for statistically significant differences ($P < 0.05$).

In RNAi experiments, transcript levels in CPB larvae were evaluated by qRT-PCR 48 h after dsRNA treatment. For each experiment, three biological replicates were analysed using the mean values of three technical replicates.

Bioassays

Cry3Aa toxicity assays were carried out in second-instar CPB larvae by voluntary feeding. Two groups of 16 larvae were placed into individual wells of 25-well boxes and starved for 2 h at 25 °C. After starvation, one group of larvae was fed with a 0.24-cm^2 disc of fresh potato leaves with a 0.6 μl drop of liquid containing 5 μg of dsRNA diluted in nuclease-free water (dsRNA-treated group) on the surface. The second group (control) was fed in the same conditions with 0.6 μl of nuclease-free water. After 2 h of treatment, both groups of CPB larvae were transferred to plastic containers with fresh potato leaves and reared at 25 °C with a photoperiod of 16:8 h (light : dark). After 48 h of treatment, CPB-ADAM10 dsRNA-treated and control larvae were fed with a 0.24-cm^2 disc of fresh potato leaves with a 0.6 μl drop of liquid containing 300 ng Cry3Aa toxin diluted in 50 mM Na_2CO_3 on the surface. As a control, CPB larvae were fed with 0.6 μl of 50 mM Na_2CO_3 in the same conditions. Upon ingestion of the entire leaf disc, larvae were fed fresh potato leaves and reared at 25 °C with a photoperiod of 16:8 h (light : dark). Mortality was recorded on day 9 after the initial dsRNA treatment. Assays were performed three times ($n = 3$).

Table 1. Primers used in quantitative real-time PCR (qRT-PCR) to analyse the expression of the Colorado potato beetle-ADAM10 metalloprotease (*CPB-ADAM10*) gene, to generate double-stranded RNA (dsRNA) in RNA interference (RNAi) experiments and to resequence the *CPB-ADAM10* coding sequence

Name	F/R	Primer sequence (5′ → 3′)	Amplicon size (bp)
qRT-PCR			
CPB-ADAM10	F	ACTCCTCGACCCGACAAAAC	81
	R	CAAGCAGATGGAACCTGTAC	
CPB-RP4	F	AAAGAAACGAGCATTGCCCTTCCG	119
	R	TTGTCGCTGACACTGTAGGGTTGA	
RNAi			
CPB-ADAM10	F	GGACTTTTGTCTCGCCTATG	465
	R	CCACAGAACGCACCAAGAG	
T7 *CPB-ADAM10*	F	TAATACGACTCACTATAGGGAGAGGACTTTTGTCTCGCCTATG	511
	R	TAATACGACTCACTATAGGGAGACCACAGAACGCACCAAGAG	
CPB-irrelevant dsRNA	F	GAGATAACGAATGGCTTCAAGG	212
	R	CAAGGTAGTTGTGTCGTGAG	
T7 *CPB-irrelevant dsRNA*	F	TAATACGACTCACTATAGGGAGAGAGATAACGAATGGCTTCAAGG	258
	R	TAATACGACTCACTATAGGGAGACAAGGTAGTTGTGTCGTGAG	
Sequencing			
CPB-ADAM10_1	F	ATGATTAGTGAATGTGTTATCGTG	456
CPB-ADAM10_456	R	CCTATTGGGGTGCGTGGTG	
CPB-ADAM10_438	F	CACCACGCACCCCAATAGG	745
CPB-ADAM10_1183	R	CATAGGCGAGACAAAAGTCC	
CPB-ADAM10_1164	F	GGACTTTTGTCTCGCCTATG	1551
CPB-ADAM10_2715	R	TCAGACTTTGTTTCTCATTTCATAGGCTCC	
CPB-ADAM10_1489	F	GCATCTGCTACTAGCGGAGATC	1226
CPB-ADAM10_2715	R	TCAGACTTTGTTTCTCATTTCATAGGCTCC	
CPB-ADAM10_438	F	CACCACGCACCCCAATAGG	1072
CPB-ADAM10_1510	R	GATCTCCGCTAGTAGCAGATGC	
CPB-ADAM10_1918	F	ACTCCTCGACCCGACAAAAC	797
CPB-ADAM10_2715	R	TCAGACTTTGTTTCTCATTTCATAGGCTCC	
CPB-ADAM10_1	F	ATGATTAGTGAATGTGTTATCGTG	1183
CPB-ADAM10_1183	R	CATAGGCGAGACAAAAGTCC	
RACE			
GSP-primer	R	CCTATTGGGGTGCGTGGTG	498
UPM-primer Clontech	F	ATTTGCTGGAGGAGCGGTG	

F, forward; R, reverse; GSP, gene-specific; RACE, rapid amplification of cDNA ends; RP4, Ribosomal protein 4; UPM, Universal Primer Mix (Clontech, Mountain view, CA, USA).

As a control, an irrelevant dsRNA (CPB-irrelevant dsRNA, Fig. S5) was synthesized for which no matches were found in a BLAST nucleotide search.

CPB-ADAM10 *coding sequence annotation*

The 5′-end coding sequence of the *CPB-ADAM10* gene was obtained by RACE with a SMARTER RACE cDNA Amplification kit (Clontech, Mountain View, CA, USA), following the manufacturer's protocol, using RNA isolated from second-instar larvae midguts. 5′-RACE first-strand cDNAs were produced by reverse transcription and used together with a gene-specific primer designed based on considering the sequence of the *CPB-ADAM10* (GSP-primer, table 1). The PCR 5′-RACE product was analysed by 1% agarose gel electrophoresis and sequenced in an ABI 3330XL Automated Sequencer (Applied Biosystems). PCR primers were designed to fill in the gap area in the *CPB-ADAM10* genome region that appears at Apollo server (Lee *et al*., 2013). The full *CPB-ADAM10* coding sequence, including the filled-in gaps and 5′-end of the coding sequence, was resequenced by the Sanger method.

Preparation of BBMVs

BBMVs were prepared from CPB larvae as described previously (Rausell *et al*., 2007) according to the method of Wolfersberger *et al*. (1987) as modified by Reuveni & Dunn (1991). BBMVs from *CPB-ADAM10* dsRNA-silenced larvae were also prepared following the same procedure.

CPB BBMV cleavage assays

Proteolysis assays on Cry3Aa were performed as described before (Rausell *et al*., 2007). Toxin (0.5 μM) was incubated with 20 μg BBMV in a final volume of 30 μl phosphate-buffered saline (8 mM Na_2HPO_4, 2 mM KH_2PO_4, 150 mM NaCl, pH 7.4) for 10 min at room temperature and centrifuged for 20 min at 12 000 *g*. The supernatant was loaded onto 10% SDS-PAGE gels and the resolved proteins were transferred onto a nitrocellulose membrane (Millipore, Billerica, MA, USA) and immunoblotted against anti-Cry3 polyclonal antibody. The secondary antibody was horseradish peroxidase-conjugated antirabbit antibody (Sigma). The immunoreactive proteins were visualized using the Western Blot Chemiluminiscence Horseradish Peroxidase Substrate detection system (Takara).

Cry3Aa toxin pore formation assays

The planar lipid bilayer technique was employed to monitor Cry3Aa toxin pore formation. Electrical bilayer measurements were performed on an Orbit-16 automated parallel bilayer platform (Nanion Technologies, Munich, Germany). Lipid bilayers

were formed on a MECA-16 microelectrode cavity array chip (Baaken *et al*., 2008, 2011) by remote liquid spreading from DPhPC (Avanti Polar Lipids, Alabaster, AL, USA) in octane as described in detail in del Rio Martinez *et al*. (2015). The reproducibility of bilayer formation was tested with at least five formation cycles of painting/electroporation at 550 mV.

The measurement chamber contained 150 μl of 20 mM Tris-HCl, pH 9.0, and 150 mM KCl. All experiments were conducted at room temperature. Bilayer array formation, BBMV fusion and insertion of the ion channels were monitored with the Orbit-16's internal multichannel patch-clamp amplifier (Triton-16, Tecella, Foothill Ranch, CA, USA). For the electrical measurements the bilayers were voltage clamped. The compartment to which the toxin or BBMVs were added was set electrical ground. The current traces were filtered with a low-pass filter at 1 kHz and recorded with a sampling rate of 5 kHz. Single-channel recordings were obtained with an Axopatch-200B patch clamp amplifier (Molecular Devices, Sunnyvale, CA, USA) that could be switched between channels using the Orbit's internal probe selector controlled by OrbitControl software (Nanion). Data were analysed using pClamp (Molecular devices). Single-channel conductance was calculated as the mean single-channel current divided by the applied transmembrane voltage.

In experiments with Cry3Aa toxin, after the bilayer array formation 1-5 μl of the toxin solution were added with gentle mixing to one side of membranes to obtain the desired Cry3Aa concentration in the recording chamber.

For fusion of the BBMVs to the preformed lipid bilayers, an aliquot of the suspension containing the BBMVs was thawed on ice, diluted to a final protein concentration of 1 μg/ml, briefly sonicated in a bath sonicator and extruded through a 200-nm polycarbonate filter. One μl of the suspension was added in close proximity to the bilayer array. A KCl-concentration gradient was created over the lipid bilayers to facilitate vesicle fusion. In cases in which too many vesicles fused, membranes were broken by applying a voltage pulse (650 mV for 200 ms) and reformed. After electrical activity was observed in at least 8 membranes on the MECA chip, the measurement chamber was rinsed with copious amounts of buffer to prevent further vesicle fusion events. Membranes displaying endogenous channel activity with conductances between 70 and 300 pS were selected for further analysis of Cry3Aa pore formation.

Acknowledgements

We thank the Genomics, Proteomics and Greenhouse Facilities of Servicios Centrales de Soporte a la Investigación Experimental (SCSIE) (University of Valencia) for technical support and Dr de la Peña for his help with the graphical representation of CPB-ADAM10 metalloprotease. We also thank Dr A. Graputto and Dr S. Schoville for inviting us to participate in the Colorado potato beetle genome analysis project and Dr M. Polchaeau for her assistance in the annotation process.

References

Abrami, L., Velluz, M.C., Hong, Y., Ohishi, K., Mehlert, A., Ferguson, M. *et al*. (2002) The glycan core of GPI-anchored proteins modulates aerolysin binding but is not sufficient: the polypeptide moiety is required for the toxin-receptor interaction. *FEBS Lett* **512**: 249–254.

Adang, M.J., Crickmore, N. and Jurat-Fuentes, J.L. (2014) Diversity of *Bacillus thuringiensis* crystal toxins and mechanism of action. *Adv Insect Physiol* **47**: 39–87.

Alonzo, F. III, Kozhaya, L., Rawlings, S.A., Reyes-Robles, T., DuMont, A.L., Myszka, D.G. *et al*. (2013) CCR5 is a receptor for *Staphylococcus aureus* leukotoxin ED. *Nature* **493**: 51–55.

Baaken, G., Sondermann, M., Schlemmer, C., Rühe, J. and Behrends, J.C. (2008) Planar microelectrode-cavity array for high-resolution and parallel electrical recording of membrane ionic currents. *Lab Chip* **8**: 938–944.

Baaken, G., Ankri, N., Schuler, A.K., Rühe, J. and Behrends, J.C. (2011) Nanopore-based single-molecule mass spectrometry on a lipid membrane microarray. *ACS Nano* **5**: 8080–8088.

Berube, B.J. and Bubeck Wardenburg, J. (2013) *Staphylococcus aureus* α-toxin: nearly a century of intrigue. *Toxins* **5**: 1140–1166.

Bischofberger, M., Iacovache, I. and van der Goot, F.G. (2012) Pathogenic pore-forming proteins: function and host response. *Cell Host Microbe* **2**: 266–275.

Bradford, M.M. (1976) A rapid and sensitive method for the quantitation of microgram quantities of protein utilizing the principle of protein-dye binding. *Anal Biochem* **72**: 248–254.

Contreras, E., Schoppmeier, M., Real, M.D. and Rausell, C. (2013) Sodium solute symporter and Cadherin proteins act as *Bacillus thuringiensis* Cry3Ba toxin functional receptors in *Tribolium castaneum*. *J Biol Chem* **288**: 18013–18021.

Dal Peraro, M. and van der Goot, F.G. (2016) Pore-forming toxins: ancient but never really out of fashion. *Nat Rev Microbiol* **14**: 77–92.

DuMont, A.L. and Torres, V.J. (2014) Cell targeting by the *Staphylococcus aureus* pore-forming toxins: it's not just about lipids. *Trends Microbiol* **22**: 21–27.

Fabrick, J., Oppert, C., Lorenzen, M.D., Morris, K., Oppert, B. and Jurat-Fuentes, J.L. (2009) A novel *Tenebrio molitor* cadherin is a functional receptor for *Bacillus thuringiensis* Cry3Aa toxin. *J Biol Chem* **284**: 18401–18410.

García-Robles, I., Ochoa-Campuzano, C., Sánchez, J., Contreras, E., Real, M.D. and Rausell, C. (2012) Functional significance of membrane associated proteolysis in the toxicity of *Bacillus thuringiensis* Cry3Aa toxin against Colorado potato beetle. *Toxicon* **60**: 1063–1071.

Gasteiger, E., Hoogland, C., Gattiker, A., Duvaud, S., Wilkins, M.R., Appel, R.D.*et al*. (2005) Protein identification and analysis tools on the ExPASy server. In *The Proteomics Protocols Handbook* (Walker, J.M., ed.), pp. 571–607. Humana Press Inc, Totowa, NJ.

Gómez, I., Oltean, D.I., Sanchez, J., Gill, S.S., Bravo, A. and Soberón, M. (2014) *Bacillus thuringiensis* Cry1A toxins are versatile proteins with multiple modes of action: two distinct pre-pores are involved in toxicity. *Biochem J* **459**: 383–396.

Gordon, V.M., Nelson, K.L., Buckley, J.T., Stevens, V.L., Tweten, R.K., Elwood, P.C. *et al*. (1999) *Clostridium septicum* alpha toxin uses glycosylphosphatidylinositol-anchored protein receptors. *J Biol Chem* **274**: 27274–27280.

Hartman, M., Herrlich, A. and Herrlich, P. (2013) Who decides when to cleave an ectodomain. *Trends Biochem Sci* **38**: 111–120.

Hua, G., Park, Y. and Adang, M.J. (2014) Cadherin AdCad1 in *Alphitobius diaperinus* larvae is a receptor of Cry3Bb toxin from *Bacillus thuringiensis*. *Insect Biochem Mol Biol* **45**: 11–17.

Inoshima, I., Inoshima, N., Wilke, G.A., Powers, M.E., Frank, K.M., Wang, Y. *et al*. (2011) A *Staphylococcus aureus* pore-forming toxin subverts the activity of ADAM10 to cause lethal infection in mice. *Nat Med* **17**: 1310–1314.

Jones, P., Binns, D., Chang, H.Y., Fraser, M., Li, W., McAnulla, C. *et al*. (2014) InterProScan 5: genome-scale protein function classification. *Bioinformatics* **30**: 1236–1240.

Krogh, A., Larsson, B., von Heijne, G. and Sonnhammer, E.L.L. (2001) Predicting transmembrane protein topology with a hidden Markov model: application to complete genomes. *J Mol Biol* **305**: 567–580.

Lee, E., Helt, G.A., Reese, J.T., Munoz-Torres, M.C., Childers, C.P., Buels, R.M. *et al*. (2013) Web Apollo: a web-based genomic annotation editing platform. *Genome Biol* **14**: R93.

Los, F.C.O., Randis, T.M., Aroian, R.V. and Ratner, A.J. (2013) Role of pore-forming toxins in bacterial infectious diseases. *Microbiol Mol Biol Rev* **77**: 173–207.

Martin, F.G. and Wolfersberger, M.G. (1995) *Bacillus thuringiensis* delta-endotoxin and larval *Manduca sexta* midgut brush-border membrane vesicles act synergistically to cause very large increases in the conductance of planar lipid bilayers. *J Exp Biol* **198**: 91–96.

Ochoa-Campuzano, C., Real, M.D., Martínez-Ramírez, A.C., Bravo, A. and Rausell, C. (2007) An ADAM metalloprotease is a Cry3Aa *Bacillus thuringiensis* toxin receptor. *Biochem Biophys Res Commun* **362**: 437–442.

Palli, S.R. (2014) RNA interference in Colorado potato beetle: steps toward development of dsRNA as a commercial insecticide. *Curr Opin Insect Sci* **6**: 1–8.

Pauchet, Y., Wilkinson, P., Chauhan, R. and Ffrench-Constant, R.H. (2010) Diversity of beetle genes encoding novel plant cell wall degrading enzymes. *PLoS One* **5**: e15635.

Peyronnet, O., Vachon, V., Schwartz, J.L. and Laprade, R. (2001) Ion channels induced in planar lipid bilayers by the *Bacillus thuringiensis* toxin Cry1Aa in the presence of gypsy moth (*Lymantria dispar*) brush border membrane. *J Membr Biol* **184**: 45–54.

Pigott, C.R. and Ellar, D.J. (2007) Role of receptors in *Bacillus thuringiensis* crystal toxin activity. *Microbiol Mol Biol Rev* **71**: 255–281.

Rausell, C., Ochoa-Campuzano, C., Martínez-Ramírez, A.C., Bravo, A. and Real, M.D. (2007) A membrane associated metalloprotease cleaves Cry3Aa *Bacillus thuringiensis* toxin reducing pore formation in Colorado potato beetle brush border membrane vesicles. *Biochim Biophys Acta* **1768**: 2293–2299.

Reiss, K. and Bhakdi, S. (2012) Pore-forming bacterial toxins and antimicrobial peptides as modulators of ADAM function. *Med Microbiol Immunol* **201**: 419–426.

Reiss, K. and Saftig, P. (2009) The "A Disintegrin And Metalloprotease" (ADAM) family of sheddases: physiological and cellular functions. *Semin Cell Dev Biol* **20**: 126–137.

Reuveni, M. and Dunn, P.E. (1991) Differential inhibition by *Bacillus thuringiensis* delta endotoxin of leucine and aspartic uptake in BBMV from midgut of *Manduca sexta*. *Biochem Biophys Res Commun* **181**: 1089–1093.

del Rio Martinez, J.M., Zaitseva, E., Petersen, S., Baaken, G. and Behrends, J.C. (2015) Automated formation of lipid membrane microarrays for ionic single-molecule sensing with protein nanopores. *Small* **11**: 119–125.

Roy, A., Kucukural, A. and Zhang, Y. (2010) I-TASSER: a unified platform for automated protein structure and function prediction. *Nat Protoc* **5**: 725–738.

Saitou, N. and Nei, M. (1987) The neighbor-joining method: a new method for reconstructing phylogenetic trees. *Mol Biol Evol* **4**: 406–425.

Takeda, S. (2009) Three-dimensional domain architecture of the ADAM family proteinases. *Semin Cell Dev Biol* **20**: 146–152.

Tamura, K., Peterson, D., Peterson, N., Stecher, G., Nei, M. and Kumar, S. (2011) MEGA5: molecular evolutionary genetics analysis using maximum likelihood, evolutionary distance, and maximum parsimony methods. *Mol Biol Evol* **28**: 2731–2739.

Thomas, W.E. and Ellar, D.J. (1983) *Bacillus thuringiensis* var israeliensis crystal delta-endotoxin: effects on insect and mammalian cells *in vitro* and *in vivo*. *J Cell Sci* **60**: 181–197.

Untergasser, A., Nijveen, H., Rao, X., Bisseling, T., Geurts, R. and Leunissen, J.A.M. (2007) Primer3Plus, an enhanced web interface to Primer3. *Nucleic Acids Res* **35**: W71–W74.

Wilke, G.A. and Bubeck Wardenburg, J. (2010) Role of a disintegrin and metalloprotease 10 in *Staphylococcus aureus* alpha-hemolysin-mediated cellular injury. *Proc Natl Acad Sci USA* **107**: 13473–13478.

Wolfersberger, M., Lüthy, P., Maurer, A., Parenti, F., Sacchi, V., Giordana, B. *et al*. (1987) Preparation and partial characterization of amino acid transporting brush border membrane vesicles form the larval midgut of the cabbage butterfly (*Pieris brassicae*). *Comp Biochem Physiol* **86A**: 301–308.

Zhu, F., Xu, J., Palli, R., Ferguson, J. and Palli, S.R. (2011) Ingested RNA interference for managing the populations of the Colorado potato beetle, *Leptinotarsa decemlineata*. *Pest Manag Sci* **67**: 175–182.

Zuckerkandl, E. and Pauling, L. (1965) Evolutionary divergence and convergence in proteins. *In Evolving Genes and Proteins* (Bryson, V. and Vogel, H.J. eds.), pp. 97–166. Academic Press, New York.

Supporting Information

Additional Supporting Information may be found in the online version of this article at the publisher's web-site.

Figure S1. Full-length Colorado potato beetle-ADAM10 metalloprotease (*CPB-ADAM10*) coding sequence annotation procedure. PCR primers were designed to fill in the gap area (red box) in scaffold 927 of the CPB genome sequence at Apollo server and to complete the 5′-end coding sequence by a 5′-rapid amplification of cDNA ends reaction (blue box).

Figure S2. Colorado potato beetle-ADAM10 metalloprotease (*CPB-ADAM10*) annotated DNA sequence and deduced amino acid sequence. Arrows delimit the prodomain, metalloprotease domain, disintegrin domain and cytoplasmic region. The signal peptide, the cysteine switch, the zinc-binding motif, the Met-turn and the transmembrane domain are underlined with solid lines. The cysteine-rich domain is dashed underlined.

Figure S3. Sequence alignment of the human ADAM10 and Colorado potato beetle ADAM10 (CPB-ADAM10) using Clustal omega (http://www.ebi.ac.uk/Tools/msa/clustalo). Protein domains, including the signal peptide, are indicated.

Figure S4. Authorship credit for organisms' pictures from Wikimedia Commons.

Figure S5. Colorado potato beetle (CPB)-irrelevant double-stranded RNA (dsRNA) synthesized using primers constructed at random, without any predetermined sequence (T7 CPB-irrelevant dsRNA, Table 1).